catalysts

MDPI

Article

Synthesis and Characterization of New Imidazole Phthalocyanine for Photodegradation of Micro-Organic Pollutants from Sea Water

Bassem Jamoussi [1], Radhouane Chakroun [1,*], Abdelmajid Timoumi [2] and Khaled Essalah [3]

1 Department of Environmental Sciences, Faculty of Meteorology, Environment and Arid Land Agriculture, King Abdulaziz University, Jeddah 21589, Saudi Arabia; bissuomaj@kau.edu.sa
2 Physics Department, Faculty of Applied Science, Umm AL-Qura University, Makkah P.O. Box 715, Saudi Arabia; timoumiabdelmajid@yahoo.fr
3 Institut Préparatoire aux Etudes d'Ingénieurs d'El Manar, Université Tunis El Manar, Unité de Recherche en Sciences Fondamentales et Didactique, Equipe de Chimie Théorique et Réactivité (UR14ES10), Tunis B.P. 244, Tunis 2092, Tunisia; khaled.essalah@gmail.com
* Correspondence: rshagroon@kau.edu.sa

Received: 11 July 2020; Accepted: 6 August 2020; Published: 8 August 2020



Abstract: In this study, a series of new metal phthalocyanines with imidazole function MPc(Imz) (M: Cd, Hg, Zn and Pd) were synthesized to improve the photocatalyst performances. All physical properties such as total energy, HOMO, LUMO energies of MPc(Imz), as well as their vibrational frequencies have been determined by DFT method using B3LYP theory level at 6-311G (d, p) and sdd basis set. The gap of energy level between work function (WF) of ITO and LUMO of PdPc(Imdz) was 1.53 eV and represents the highest barrier beneficial to electron injection compared to WF of ZnPc(Imz), HgPc(Imz), and CdPc(Imz). Furthermore, the PdPc(Imdz) thin films on indium tin oxide (ITO) glass were prepared by spin coating and vacuum evaporation technique, and were characterized by X-ray diffraction (XRD), surface electron morphology (SEM), atomic force microscopy (AFM), and UV–Vis spectroscopy. The photocatalytic activity of the ITO/glass supported thin films and degradation rates of chlorinated phenols in synthetic seawater, under visible light irradiation were optimized to achieve conversions of 80–90%. Experiments on synthetic seawater samples showed that the chloride-specific increase in photodegradation could be attributed to photochemically generated chloride radicals rather than other photoproduced reactive intermediates [e.g., excited-state triplet PdPc(Imz) (^{3}PdPc(Imz)*), reactive oxygen species]. The major 2,3,4,5-Tetrachlorophenol degradation intermediates identified by gas chromatography-mass spectrometry (GC/MS) were 2,3,5-Trichlorophenol, 3,5-dichlorophenol, dichlorodihydroxy-benzene and 3,4,5-trichlorocatechol.

Keywords: metal phthalocyanine; new imidazole; photodgradation; DFT method; seawater; catalysis

1. Introduction

Chlorophenols are widespread environmental pollutants and professional contaminants formed following the disinfection of water rich in organic matter residues by chlorination process [1] or by the degradation of organochlorine pesticides [2]. These compounds which are widely used in the chemical industry and in agriculture are known for their high toxicity and environmental persistence and bioaccumulation in the food chain [3,4]. Metal complexes of phthalocyanine compounds (MPcs) have received increased attention in recent years from researchers due to their chemical and thermal properties and its versatile application in various fields of applied research, including photovoltaic cells [5], gas sensors [6], photodynamic therapy of cancer [7], semiconductor display devices [8,9], liquid crystal [10] and homogeneous or supported catalysts [11,12] allowing an environmentally

friendly degradation of organic pollutants in water. Some photocatalysts such as cobalt (II) 2,9,16,23-tetrasulphophthalocyanine (CoTSPc) have been used in the sweetening process "Merox process" to remove a major part of mercaptans from petroleum products [13] and photodegradation of organic dyes in aqueous solutions under visible light [14]. In addition, it is well known that iron phthalocyanine (FePc) complexes have been extensively investigated as catalysts for epoxidation of a number of olefins [15–17] and oxidation of aromatic compounds [18], bleaching treatment of pollutants in water [19–21], and chlorinated phenols in aqueous solutions under mild conditions [22–25]. Particular attention has been paid by our research team to degradation of pollutants with a high pollution potential such as nitroaromatic pollutants [26] and hydroxytyrosol in olive oil mill wastewaters, using zinc phthalocyanine modified titanium dioxide after irradiation with solar light [27]. One of the inherent drawbacks of phthalocyanines is their low solubility in most organic solvents. This problem can be addressed by anchoring appropriate peripheral substituents to the ring system [28]. The choice of substituents is not intended only to improve the solubility of MPcs, but also to adjust the catalytic properties by modifying the electron attractor or electron donor character of the substituents. In order to avoid the profound effect on the stability of phthalocyanine by nucleophilic, electrophilic, and radical attacks, the introduction of the imidazole moieties into phthalocyanines is one of the convenient solutions to maintain the electron transfer processes [29]. Encouraged by this information, we report the preparation of new phthalocyanines (Pcs) with imidazole functions Pc(Imz), which give properties to the core system suitable for application in photo catalysis. The compounds obtained are then used for the preparation of novel Pcs(Imz) thin film prepared by spin coating to determine whether they have the properties required for the intended application. Recently, very interesting research on methods of immobilizing MPcs on various supports with different work function (WF) has become one of the attractive fields for many researchers to improve the catalytic activity often used in the decontamination of pollutants. In this study, ITO is used as active substrate. This support has been chosen because the energy-level gap between WF of ITO and LUMO of PdPc (Imz) (i.e., 1.5 eV) is larger than that of LUMO of PdPc(Imz) and WF of other commonly used active substrates (e.g., Cu [30], Ag [30], TiO_2 [31]). This higher electron injection barrier of PdPc(Imz)/ITO should make electron injection into the ITO acceptor easier and faster, which may contribute to the separation of electron–hole pairs and release more holes and electrons in the chlorophenols' degradation reaction. Indeed, Xu et al. [32] showed that the photocatalytic degradation of Rhodamine B dye using iron phthalocyanine was influenced by the nature of the substrate and the film thickness. Several approaches have been proposed to enhance the photocatalytic process by immobilizing MPcs on different supports using various methods including grafting, anchoring, and electrostatic process. However, only few papers have reported fabrication of MPcs thin films using spin coating technique as photosensitizer for the photodegradation of micro-organic pollutants in chlorinated water [32–35].

In this paper, zinc tetra(1H-imidazol-1-yl)phthalocyanine (ZnPc(Imz)) powder was used as a starting material to fabricate ZnPc(Imz) thin films onto glass substrates by spin coating method. Furthermore, thin films were characterized by means of X-ray diffraction (XRD), infrared spectroscopy (FTIR), and UV–Vis spectroscopy. Thin films deposited on glass substrates were used for the degradation of chlorinated phenols mixture (2-Chlorophenol (2-CP), 2,4-Dichlorophenol (2,4-DCP), 2,4,6-Trichlorophenol (2,4,6-TCP) and 2,3,4,5-Teetrachlorophenol (2,3,4,5-TeCP)) spiked in synthetic seawater using a visible halogen-lamp as a light source in a photoreactor. The photoreactor used has been newly designed in our laboratory by making some small modifications to the device used in our previous studies [26,27]. The effects of initial chlorinated phenols mixture concentration, pH solution, and catalyst dosage on the photodegradation of each component of chlorinated Phenols Mixture were also investigated. Reaction intermediate components were identified by gas chromatography-mass spectrometry (GC-MS). The advances brought by our work include the enhancement of the photodegradation of specific classes of chlorinated phenols in artificial sea water. In this regard, we found that photochemically generated chloride radicals play a more prominent

role in photodegradation than other photoproduced reactive intermediates [e.g., excited-state triplet PdPc(Imz) (^{3}PdPc(Imz)*), reactive oxygen species].

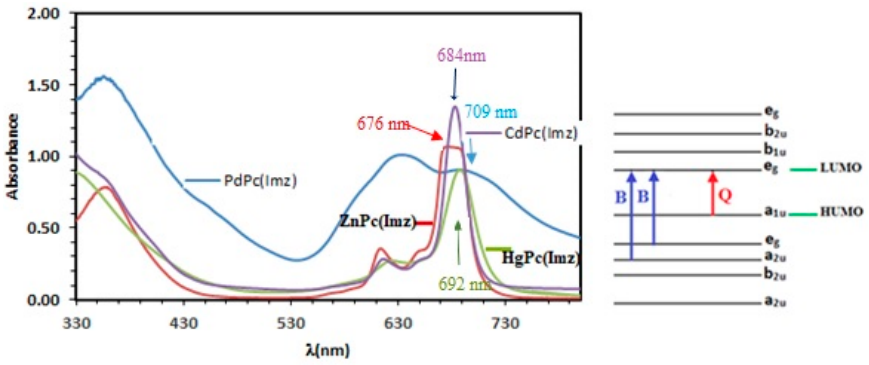
2. Results and Discussion

2.1. UV–Vis Spectrum of Metallophthalocyanines (M: Zn(II), Cd(II), Hg(II) and Pd(II))

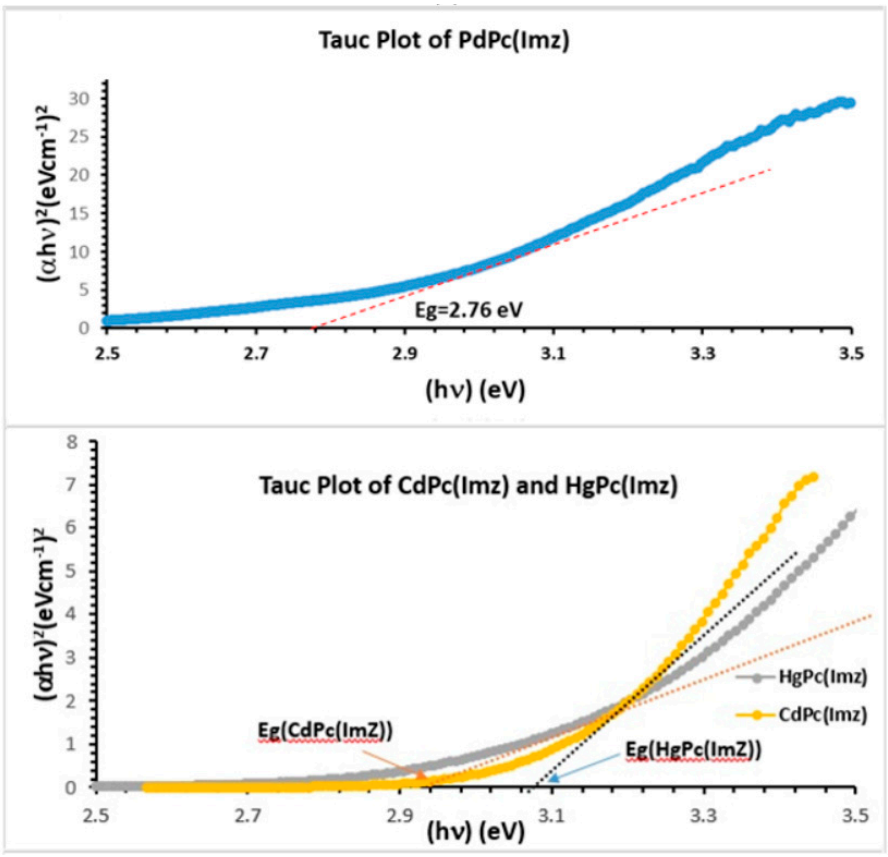
The absorption spectra of ZnPc, CdPc, HgPc, and PdPc show two typical main absorption bands of phthalocyanines. The first is the B (or Soret) band, between 300 and 400 nm, and the other is the Q band, observed between 600 and 750 nm [36]. The B band results from the transition between (a_{2u}) and (e_g) lowest unoccupied molecular orbital (LUMO), whereas the Q band mainly involves a charge transfer from the pyrrolic carbons to the other atoms of the molecule. The visible region is associated to π–π** transition of the conjugate system doubly degenerated transition (a_{1u}-e_g) from the highest occupied molecular orbital (HOMO) to the lowest unoccupied molecular orbital (LUMO) [37]. The splitting of the peaks observed in the Q-band region may be associated to the dimeric species in solution. In addition, the Q band is strongly affected by the nature of the diamagnetic metal, which plays a role in the shift of the Q band towards the red "redshift". As cited in the literature [38], the ionic radius of the metal cation in the ligand influences the size of the ligand, which can be explained by the increase in electron density. This was verified for the studied MPcs (Figure 1a), as the mercury has an ionic radius of 110 pm, which is greater than cadmium (95 pm), zinc (74 pm), and palladium (64 pm). On the other hand, the more the metal ion is electronegative, the more the displacement of the Q band towards longer wavelengths is favored, which is in good agreement with the Pauling electronegativity scale (χ_r), on a relative scale running from 1.65 (zinc) to 2.2 (palladium). Leznoff et al. [39] reported that Phthalocyanines with diamagnetic metal ion provided high singlet oxygen quantum yields and efficient photodegradation of pollutants. The interaction of the excited triplet state of the MPc with ground-state molecular oxygen provides hydroperoxyl ions, which allow oxidation of pollutants [40]. Compared to zinc phthalocyanine, Cd, Hg, and Pd-substituted metalphthalocyanines display bathochromic shifts ranging from 8 nm to 33 nm. It is to be noted that the Q band absorption is sensitive to central metals of the Pc macrocycle. The Q-band absorptions of ZnPc(Imz), CdPc(Imz), and HgPc(Imz) are at 676 nm, 684 nm, and 692 nm, respectively, but PdPc(Imz) has a maximum absorption at 709 nm, which corresponds to 33 nm red-shift. According to the literature, it is well known that palladium and its complexes are widely used in homogeneous and heterogeneous catalysis [41].

We must also emphasize that the substituted palladium phthalocyanines having Q band absorptions shifted to the red region may be explained by the enhancement of the catalytic activity of palladium following the cumulative effect of the metal ion and the phthalocyanine core. The presence of peaks at high photon energies indicated the association of the d-electrons of the central metal in the electronic transition. The shift of absorption maxima depends upon the change in electron distribution and the size of the macrocycle. As shown in Table 1, energy gap experimentally varies in the following order: ZnPc(Imz) < CdPc(Imz) < HgPc(Imz) < PdPc(Imz). According to the optical gap, it can be expected that the Q bands whose wave-lengths are in inverse order of the gap would follow the trend of ZnPc(Imz) > CdPc(Imz) > HgPc(Imz) > PdPc(Imz). In other words, a hypsochromic shift of the absorption band occurs progressively from ZnPc(Imz) to PdPc(Imz). On the other hand, the electronegativity according to Pauling (χ) for the central M are in the sequence of Pd (2.2) > Hg (2.0) > Cd (1.69) > Zn (1.65). The Pd has the smallest positive charges, which makes it less likely to lose its electrons and consequently has the most stable electron configuration among the studied metals: (Ar) $3d^{10}4s^2$ for Zn, (Kr)$4d^{10}5s^2$ for Cd, (Xe)$4f^{14}5d^{10}6s^2$ for Hg, and (Kr) $4d^{10}5s^0$ for Pd. Most studies have focused on interpreting UV-vis spectra to study the different *nd* series of diamagnetic metal-phthalocyanines and their excited states in order to select the best metal phthalocyanine, which has good electrocatalytic activity and stability for the oxidation of organic compounds, leading to a high rate of singlet oxygen ratio. To our knowledge, no study has been

undertaken on the effect of nd^{10}metal Pcs (e.g., $3d^{10}$: ZnPc; $4d^{10}$CdPc; $5d^{10}$: HgPc; $6d^{10}$: PdPc) on the sensitivity and selectivity of their films towards different analytes (chlorophenols in this study).



(**a**)



(**b**)

Figure 1. (**a**) UV-Vis spectra showing two characteristic bands of phthalocyanine: B bands at 352, 361 and 380 nm respectively, and Q bands at 680, 683 and 690 nm respectively. (**b**) Band gap (Eg) determination, using Tauc plot extrapolation.

Table 1. Values of optical band gaps of MPc(Imz) (M: Zn; Hg; Cd; Zn; Pd).

Optical Band Gaps				
MPc(Imz)	HgPc(Imz)	CdPc(Imz)	ZnPc(Imz)	PdPc(Imz)
Optical band gap (eV)	2.94	2.87	2.83	2.76

2.2. FT-IR Study of Metallophthalocyanines (M: Zn(II), Cd (II), Hg(II), and Pd(II))

FT-IR spectra have been made for CdPc(Imz), HgPc(Imz), ZnPc(Imz), and PdPc(Imz) synthesized in this work (see Supplementary Materials). FT-IR results indicate a high stability of the metal phthalocyanines and corroborate UV–vis analysis. Detailed IR spectra analysis is provided in Supplementary Materials.

The analytical data for all metallophthalocyanines were in good agreement with the proposed structures. It can be believed that the PdMPc(Im) could be a promising catalyst for application in photocatalytic degradation under visible-light due its lower HOMO-LUMO energy gap (~2.2 eV).

The Optical Band Gap of Tetra [4-(1H-imidazol-1H-imidazol-1-yl)] MPcs (M: Cd, Zn, Hg, Pd)

To find out the value of the optical band gap for semiconductor nanostructures [42,43], thin films [44], and liquids [45], Tauc plot is tremendously used. In the present study, Tauc plot was used to find out the value of the optical band gap of solutions containing MPc(Imz). Tauc plot is deduced from Figure 1a, and linear parts of the curves are extended to intersect with energy axis. The intersection point provides the value of the optical band gap Eg (Figure 1b). A substantial variation is observed in the value of indirect optical band gap of MPc(Imz) (M: Pd, Cd, Hg) (Table 1) when the same amount of MPc(Imz) was dissolved in DMSO. Among all solutions used in the present study, HgPc(Imz) solution showed highest value of the indirect optical band gap (2.94 eV), compared to CdPc(Imz) (2.87 eV) and PdPc(Imz) (2.76 eV) solutions. These optical bands Eg were determined from the analysis of the absorption spectrum as described by Tauc plot using the formula [46,47]:

$$\alpha h\nu = \alpha_0 (h - Eg)^n \quad (1)$$

where hν is the energy of incident photons and Eg is the value of the optical band gap corresponding to transitions indicated by the value of n (n = 1/2 for direct transition and n = 2 for indirect transition). α_0 is the Tauc coefficient describing the efficiency in light absorption [42,48]. From Table 1, we can notice that the energy of the gap of CdPc, HgPc, and ZnPc are much larger than PdPc, which causes for them some limitation to effectively absorb the visible light. We then chose to use PdPc for the remainder of the study.

The geometric optimization of PdPc using the Gaussian W program (detailed in Supplementary Materials) shows a planar structure (Figure 2).

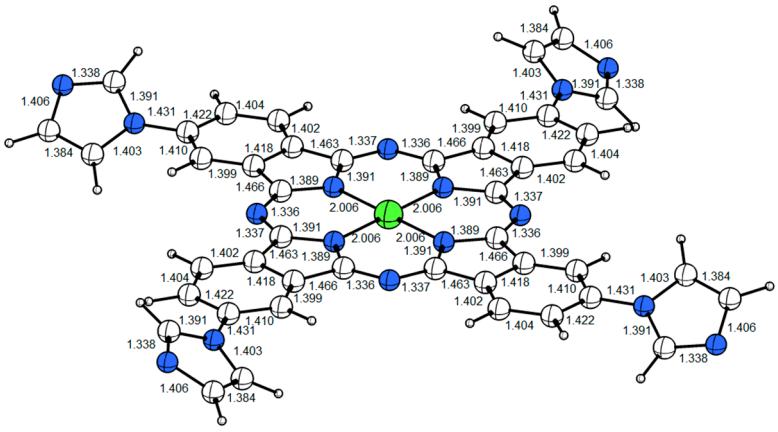


Figure 2. The planar structure of the palladium phthalocyanine PdPc molecule. The Pd and N atoms are respectively labeled in green and blue. The Pd–N bond length of the optimized structure is 2.006 Å.

In the Q-band, the electronic transition occurs from HOMO, which has an electronic density mainly located on the phthalocyanine molecule, to the LUMO, which has a small electronic density on Pd–N bond as shown in Figure 3. The calculated energy gap (HOMO-LUMO) is Eg = 2.23 eV.

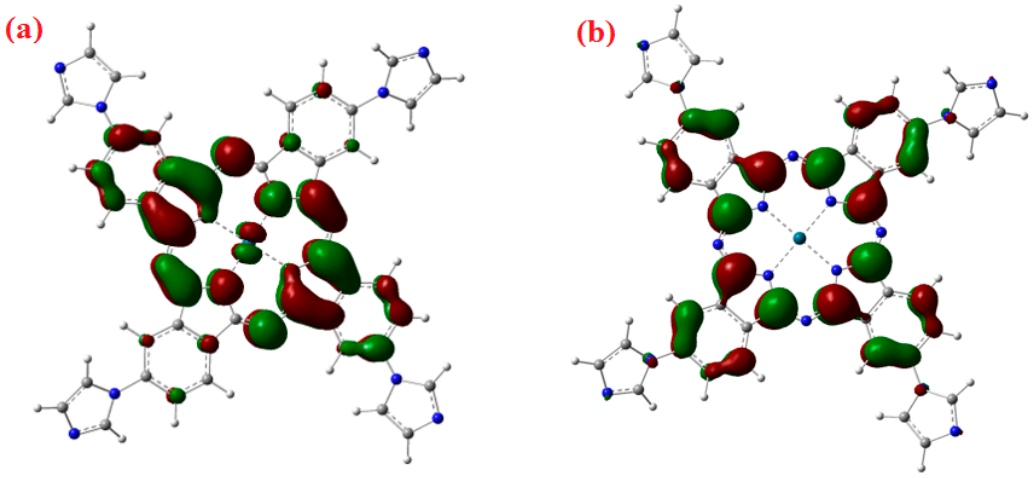


Figure 3. Virtual (**a**) LUMO and (**b**) HOMO orbital frontiers of PdPc molecule, the theoretical energy gap is 2.26 eV.

2.3. Preparation and Characterization of Photo-Catalytic PdPc Thin Films

The synthesis of palladium (II) phthalocyanine (PdPc) has been extensively presented in our previous work [49]. The films were deposited at room temperature, by vacuum thermal evaporation onto 1 mm thick rectangular ITO/glass substrate. The structure of the PdPc thin films was studied using X-ray diffraction (XRD) technique. The diffraction spectra were measured at 2θ scanning ranging from 0 to 90 degrees diffraction angle. Figure 4a shows the XRD spectrum of ITO (JCPDS card no. 6-0416) [50] and PdPc thin films deposited on ITO. The XRD spectrum of the ITO sample is characterized by peaks at 21.03, 30.27, 35.16, 50.55, and 60.16 from indium tin oxide, a polycrystalline ITO substrate [51] of cubic crystalline ITO [52]. For the PdPc films deposited by vacuum thermal evaporation technique, a new peak appears at 43.98 besides the peaks from the ITO substrate.

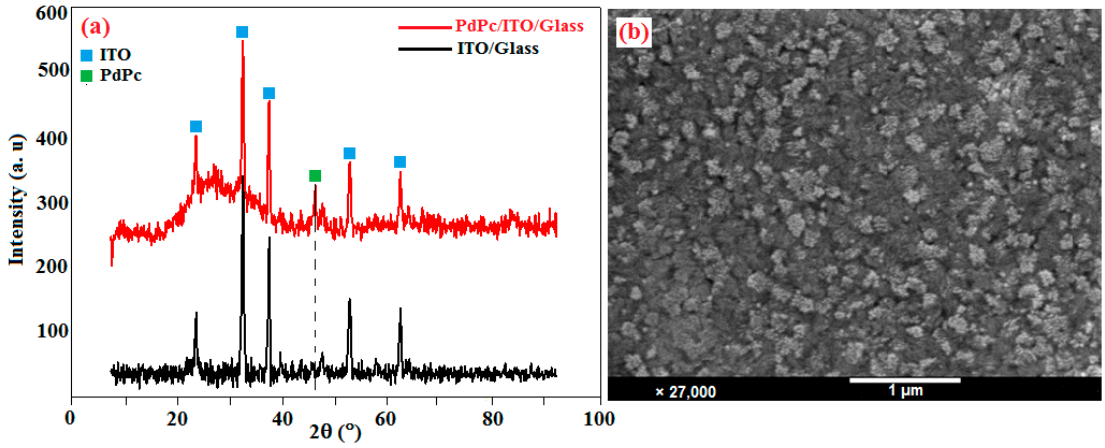


Figure 4. (**a**) XRD spectra and (**b**) SEM image of PdPc thin films grown by vacuum thermal evaporation technique on ITO/glass substrate.

A plan view scanning electron microscopy (SEM) micrograph of the PdPc thin films deposited on ITO/glass substrate at 300 K is shown in Figure 4b. The SEM image shows that the sample surface is completely covered with nanosized PdPc spherical particles. The film was also covered with uniformly distributed grains having different shapes without any cracks. The SEM micrograph reveals a uniform rough surface with no clear crystal grain structure. The EDX pattern confirms the presence of only C, O, N, and Pd in the sample.

Figure 5a shows the 3D AFM image for an area of 5 µm × 5 µm of the palladium phtalocyanine thin film surface. The image exhibits a rough surface, with forms that might indicate that phthalocyanine molecules grew in aggregation rows, rather than in the parallel or in the zig-zag arrangement. This suggests that the roughened surface of the thin film would be due to growth mechanism of the technique. Figure 5b shows the transmittance data of the prepared PdPc/ITO thin film in the range of 200–1800 nm. The most important feature in this figure is the shift of the absorption band edge toward the lower wavelengths. This shift is translated as optical band gap enlargement. Furthermore, a high absorption region can be noted at wavelengths $\lambda < 350$ nm, allowing energy gap value adjustment. A direct energy gap is observed for PdPc, whereas for a semiconductor with indirect gap, it is degraded. A second high transparency region is also observed at $\lambda > 350$ nm, giving a transparent character to the thin layers.

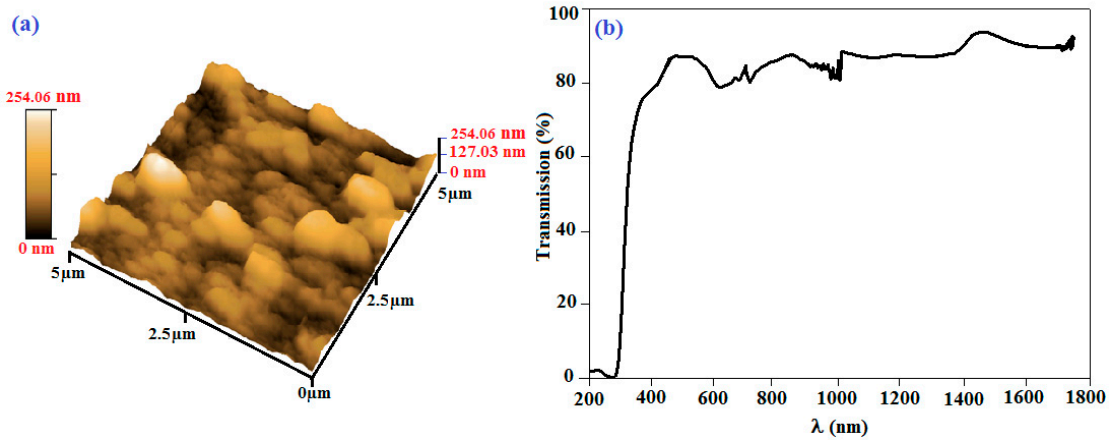


Figure 5. (**a**) 3D AFM image and (**b**) variation of transmission as function of wavelength for PdPc thin films grown by vacuum thermal evaporation technique on ITO/glass substrate.

2.4. Photocatalysis

2.4.1. Effect of Initial pH and Initial Concentration

The extent of compound degradation by PdPc(Imz)/ITO/Glass in the presence of great amount of oxygen was found to be highly dependent on pH and initial chlorophenols' concentration $[CPs]_0$. The control of chlorophenols' decomposition as well as the intermediates and final products identification has been realized using gas chromatography–mass spectrometry (GC-MS). In this part of the study, we focused on the optimization of photocatalytic degradation of some chlorophenols using Response Surface Methodology (RSM), based on statistical design of experiment evaluation in which two parameters are varied simultaneously. The influence of parameters (initial pH and initial concentration for each chlorophenol) was investigated by employing experimental design with 2^3 level factorial design 2^3. The results are reported in Supplementary Materials.

2.4.2. Photocatalytic Mechanism of PdPc(Imz)

Based on the results discussed above, the proposed photocatalytic mechanism of chlorophenols degradation using PdPc(Imz)/glass thin film in the presence of oxygen and under visible light irradiation is illustrated in Figure 6. Work function (WF) of investigated glass was between 4.4 eV–4.80 eV as reported elsewhere [53]. The luminescence center is explained by the oxygen vacancy model and by interlobular oxygen bound by the ionized silicon atom [53].

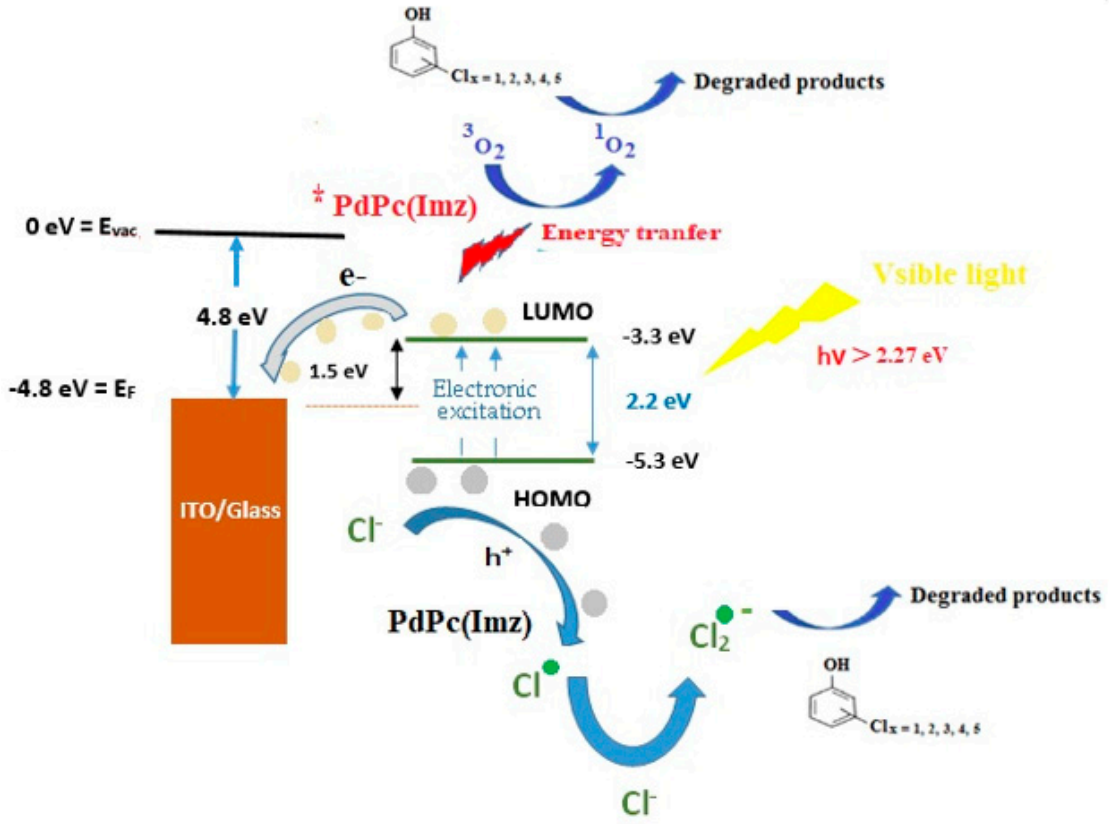


Figure 6. Schematic of electron-hole pairs separation at the interface of PdPc(Imz) films deposited on glass substrate under visible light irradiation in artificial seawater.

The calculated energy gap of PdPc(Imdz) was 2.26 eV, the lowest unoccupied molecular orbital (LUMO) of PdPc(Imdz) was (−3.27 eV), and the highest occupied molecular orbital (HOMO) of PdPc(Imdz) was (−5.54 eV). As reported in the literature [54,55], the height of the electron injection barrier depends on the difference between WF of the cathode and the energy level of the polymer. A higher barrier is favorable for the injection of electrons. The energy–level gap between WF of Glass and LUMO of PdPc(Imdz) in the system was 1.53 eV and the higher electron injection barrier played a part in the separation of electron-hole pairs and released more electrons and holes in the chlorophenols degradation reaction. It is assumed that the electron-hole pair separation efficiency plays a key role in the photocatalytic reaction [56]. Visible light irradiation generates electrons which can reduce O_2 to O_2 radicals. On the other hand, holes can oxidize OH^- to •OH. The number of radicals produced depends on the efficiency of electron–hole pair's separation (Figure 6). It has been reported in the literature [54–56] that all these radicals (O_2 and OH, and $^1O_2$) could be responsible for chlorophenols degradation.

In most studies, the reaction mechanism and the active species assumed to be involved in the photodegradation reaction are based on the results obtained from experiments carried out in deionized water or in aqueous solutions with low chloride concentration. In order to validate the hypothesis of the corresponding photochemical pathways, a series of experiments was conducted in synthetic water matrices containing only 20 mM phosphate buffer at pH = 8 to isolate or quench specific reaction pathways. Common scavengers were used for trapping experiments such as methanol as a hole scavenger h+, isopropyl alcohol (IPA) as a scavenger (•OH) (and $AgNO_3$ as electron scavenger (e^-), while 1,4-Diazabicyclo[2.2.2]-octane (DABCO) have been used to quench singlet molecular oxygen $^1O_2$. Application of 25 mM of methanol as a radical quencher resulted in a high reduction in chlorophenols' photodegradation. Similarly, a moderate contribution of e- to chlorophenol degradation resulted from application of 25 mM of $AgNO_3$. An additional test was conducted using 50 mM of

1,4-Diazabicyclo[2.2.2]-octane (DABCO) [55], which indicated low contribution of $^1O_2$ to chlorophenols' photodegradation and suggested that $^1O_2$-mediated pathways are not the dominant contributors to chlorophenols' photodegradation in synthetic water matrices containing 20 mM phosphate buffer. These results confirmed the assumptions reported in the literature [56–58]. The sensitization process increased the photocatalytic yield due to new possible routes for generating more active species following three steps:

$$PdPc(Imz) + h\nu \rightarrow {}^3[PdPc(Imz)]^* \quad (2)$$

$$^3[PdPc(Imz)]^* + {}^3O_2 \rightarrow PdPc(Imz) + {}^1O_2\ (^1\Delta) \quad (3)$$

Following absorption of visible light, the thin film PdPc(Imz)/ITO/Glass is promoted to the excited triplet state ^{3}[PdPc(Imz)]* (Equation (2)), and could react with molecular $^3O_2$ (Equation (3)), leading to the excited singlet molecular oxygen (O_2-$^1\Delta$g) and forming an excited state complex (exciplex). The molecular oxygen quenching by chlorophenols (CPs) involved an intermediate with partial charge transfer according to Equation (4):

$$CPs + {}^1O_2 \rightarrow [CPs \ldots \ldots {}^1O_2] \rightarrow \text{Degraded product} \quad (4)$$

However, high chloride concentration is the key characteristic distinguishing artificial seawater from low or free chloride aqueous solutions. Indeed, chlorides are the predominant sink for •OH in seawater, with Cl− scavenging (Equation (5)), resulting in decreased •OH concentrations:

$$\bullet OH + Cl^- \rightarrow Cl\bullet + OH^- \quad (5)$$

It appears clearly that some important reactive intermediates in aqueous solution (including •OH) would play a less prominent role in PCs photodegradation in artificial seawater (Figure 6).

2.5. Kinetic Evaluation

The photocatalytic activity of thin films of PdPc(Imz)/ITO/Glass for removing the chlorophenol compounds (2-CP, 2,4-DCP, 2,4,6 -TCP and 2,3,4,5-TeCP) from aqueous solution follows the pseudo-first-order kinetic model. The simplified kinetic model equation [56] describing first-order kinetics is given as:

$$\ln \frac{[CP]_0}{[CP]_t} = k_{obs}t, \quad (6)$$

where k_{obs} represents the apparent rate constant, $[CP]_0$ is the initial concentration (mg·L^{-1}), $[CP]_t$ is the t time concentration. By plotting $\ln([CP]_0/[CP]_t)$ versus irradiation time, a straight line was observed for all compounds with a slope of k_{obs} (Figure 7).

The initial rate of photocatalytic degradation (r_0), first order rate constants for degradation (k_{ob}), correlation coefficients, and half-lives ($t_{1/2}$) at various initial concentrations of each chlorophenol are summarized in Table 2.

Table 2. First–order rate constant (k_{ob}), initial rate of photocatalytic degradation (r_0), correlation coefficients and illumination times during which 50% ($t_{1/2}$) or 99% ($t_{99\%}$) of pollutant are degraded.

Pollutant	k_{obs} (min^{-1}) × 10^3	r_0 (μmol min^{-1})	$t_{1/2}$ (min)	$t_{99\%}$ (min)	R^2
2-CP	38	1.26	18.24	121.18	0.9989
2,4-DCP	156	3.10	4.44	29.52	0.9968
2,4,6-TCP	27	0.67	25.67	170.56	0.9966
2,3,4,5-TeCP	21	0.40	33.00	219.29	0.9974

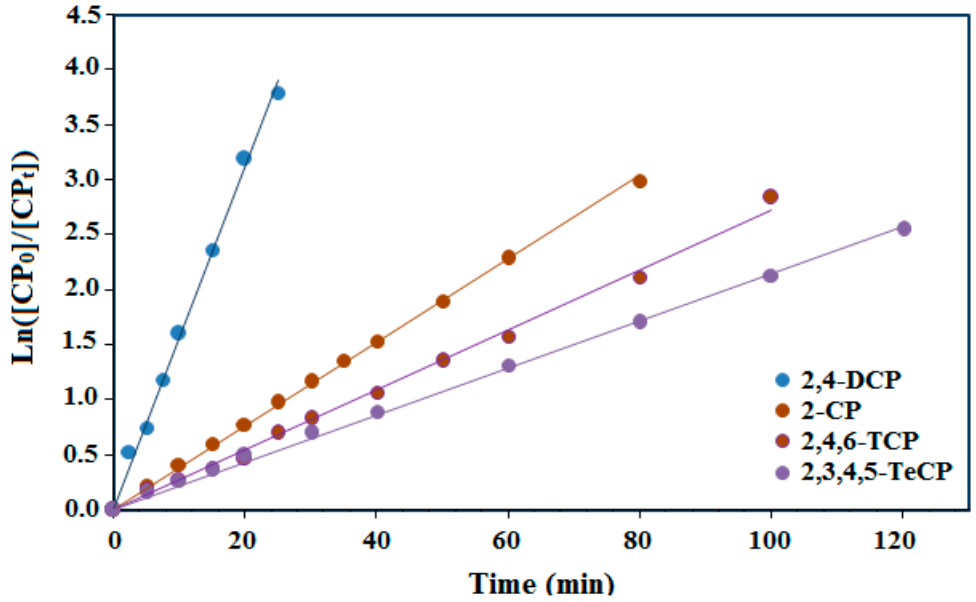


Figure 7. The kinetics model of photodegradation performance of the thin film PdPc(Imz)/ITO/glass at pH8.

All of the four experiments showed a good fit for the pseudo-first-order model. However, the 2,4-DCP photocatalytic experiment with an initial concentration of 5 mg L^{-1} (39 µmol min^{-1}) had a better fit than the other chlorophenols (2-CP, 2,4,6-TCP and 2,3,4,5-TeCP). Based on the results depicted in Table 2 and Figure 7, it can be concluded that the reactivity of the chorophenols decreases with the increasing number of chlorine atoms on the aromatic ring. The first order degradation rate constants (k_{ob}) may be influenced by the interaction of the chlorine electron withdrawing and the steric effect of the chlorine, which can block some favorable positions susceptible to the hydroxyl radical attack. For tetra-chlorophenols (2,3,4,5-TeCP), steric hindrance plays an important role during their dechlorination process. Indeed, the dechlorination process is all the more difficult as the chlorine atoms are closer to each other on the aromatic cycle. The rate constant value of 2,3,4,5-TeCP obtained at pH = 8 ($k_{obs} = 20 \times 10^{-3}$ min^{-1}) is in good agreement with the results obtained at pH 11 by Czaplicka et al. [59] ($k_{obs} = 18.3 \times 10^{-3}$ min^{-1}). Moreover, the oxidation of the monochlorophenols was faster than that of the trichlophenols and tetrachlorophenols, but less easy than the dichlorophenols. Figure 8 shows the photocatalytic degradation of each chlorophenol during different illumination times and in the presence or the absence of the photocatalyst (PdPc(Imz)/ITO/glass thin films). This photocatalyst did not exhibit any photoactivity in the dark, neither in the absence nor in the presence of oxygen (Figure 8), suggesting that it is necessary to photoexcite the photosensitizer (PcPd(Imz)). Furthermore, the increase of the number of chlorine atoms has a significant effect on the initial rates (r_0) as well as the degradation rate constants (k_{obs}). The values of (r_0) for 2,4-DCP, 2-CP, 2,4,6-TCP and 2,3,4,5 TeCP were 3.10, 1.26, 0.67, and 0.40 µmol min^{-1}, respectively. This can be explained by the fact that the excited molecules have different polarizations.

Following photocatalytic treatment of chlorophenols' mixture (2-CP, 2,4-DCP, 2,4,6-TCP and 2,3,4,5-TeCP) at equal initial concentration $[CP]_0$ = 5 mg/L, an increased overlap of chromatographic peaks was observed. Therefore, many difficulties to follow the degradation of the chlorophenols' mixture from a chromatographic analysis have arisen (Figure 9).

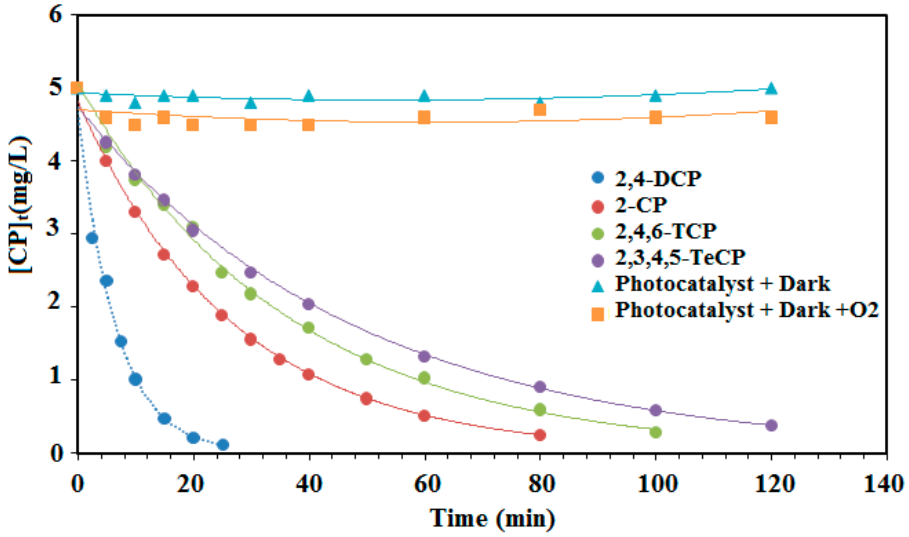


Figure 8. Effect of illumination times on the initial rates of separate photocatalytic degradation (r_0) of chlorophenols (2-CP, 2,4-DCP, 2,4,6-TCP and 2,3,4,5-TeCP). (The initial concentration of each phenol 5 mg/L, at pH = 8.)

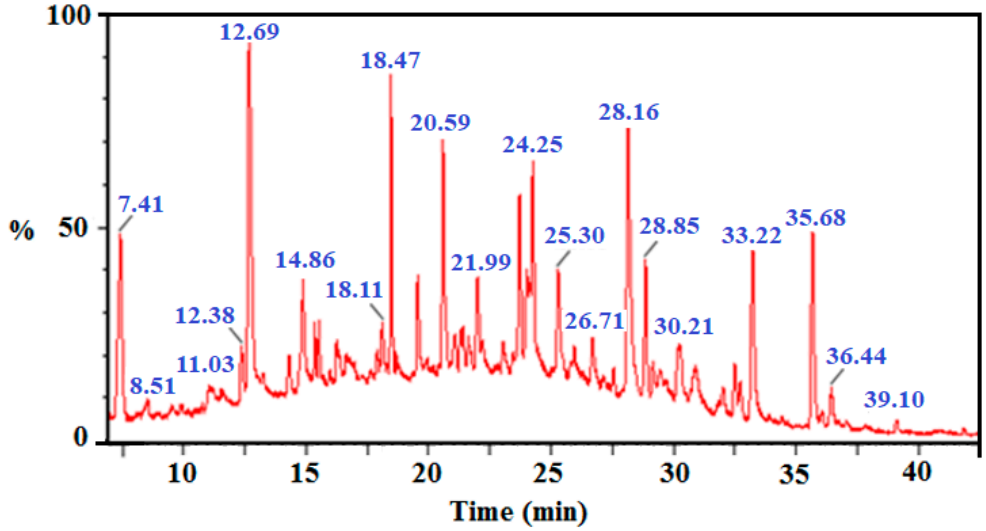


Figure 9. Total ion chromatogram of mixture of four chlorphenols (2-CP, 2,4-DCP, 2,4,6-TCP and 2,3,4,5-TeCP) after 120 min illumination time.

In fact, these four reactants and their degradation intermediates compete to react with the free radicals generated during the illumination of the PdPc(Imz) thin film, so that changes in the kinetics (Figure 10) are not unexpected in comparison with individual degradation. It is therefore difficult to predict the degradation kinetics for a mixture of several chlorophenols in water. Based on the obtained results, we may conclude that the chlorophenols' mixture has a significant influence on the initial reaction rate for each single chlorophenol. This effect has a very similar tendency for the four chlorophenols within the studied pH region, but its influence on the initial rate turns out to be different. In all cases, our results suggest that over a relatively wide pH range, the efficiency of the process is mildly affected, which is interesting as the process could be applied to different types of water.

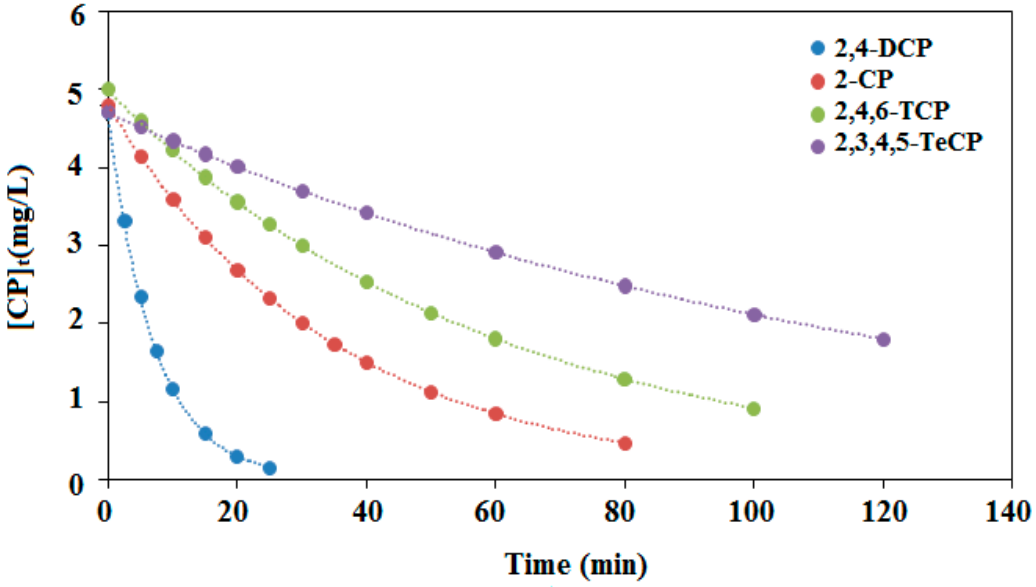


Figure 10. Effect of illumination times on the initial rates of photocatalytic mixture degradation (r_0) of chlorophenols (2-CP, 2,4-DCP, 2,4,6-TCP and 2,3,4,5-TeCP). (The initial concentration of each phenol 5 mg/L, at pH = 8.)

2.6. Intermediates from the Photodegradation of Chlorophenols

Various reaction by-products formed during the degradation of monochlorophenols [60,61], dichlorophenols [56,62] and trichlorophenols [62] have been previously studied in detail. The main by-products identified include phenols, quinones, catechols, chlorohydroquinone, and hydroxyhydroquinone. Furthermore, many of the degradation pathways and mechanisms have been proposed, involving a sequence of hydroxylation, giving some intermediate compounds, which are subsequently degraded via ortho-, or meta-cleavage pathway through the formation of short-chain aldehydes and carboxylic acids. Finally, the short-chain aldehydes and carboxylic acids are transformed into CO_2 and H_2O by a decarboxylation mechanism [63–65]. Although a large number of papers treated the subject of degradation by-products of various chlorophenols, studies on 2,3,4,5-tetrachlorophenol photodegradation remain very few [59]. This can be explained by the fact that 2,3,4,5-TeCP has more Cl atoms on the aromatic ring especially at the ortho- and para- positions, which makes it more stable and more difficult to photodegrade.

In order to have information on the main degradation by-products of 2,3,4,5-TeCP, GC/MS technique was employed. All data were acquired with an Agilent 6890-5973N GC/MS system in a raw (profile) scanning mode and followed by NIST MS Database Search and elemental composition determination by Mass Works library. Figure 11b gives major reaction intermediates including trichlorophenols as 2,4,5-TCP, 2,3,5-TCP, 3,4,5-TCP, and trichlorocatechol. Some dichlorophenols as dichlorodihydroxy-benzene and 3,5-DCP have also been identified.

Given the intermediate products identified by GC-MS, we suggest the following degradation mechanism: After hydroxyl radicals' formation following electron transfer from OH- groups to the PdPc(Imz) photoexcited surface, the hydroxyl radicals attack 2,3,4,5-TeCP, converting it to 3,4,5-trichlorocathechol and then to dichlorodihydroxy-benzene. The 2,3,4,5-TeCP can also be dechlorinated to give a mixture of 2,3,5-TCP, 2,3,4-TCP and 3,4,5-TCP, which then can be for a second time dechlorinated to give 3,5-DCP.

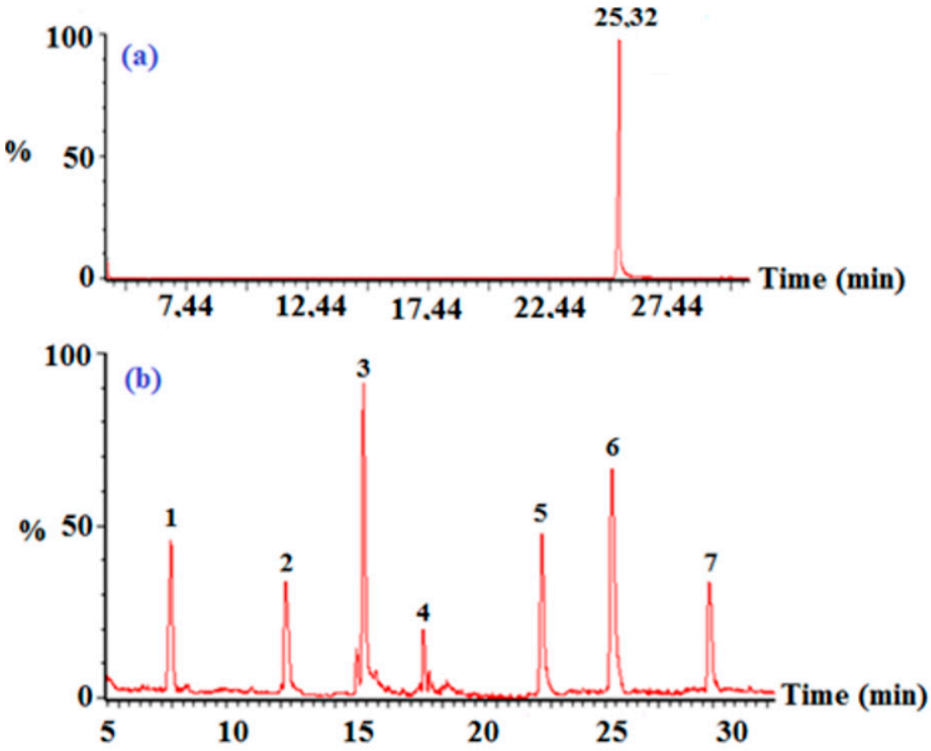


Figure 11. (**a**) Total ion chromatogram of 2,3,4,5-TeCP at t = 0; and (**b**) after 120 min illumination time: (1) 2,3,5-TCP, (2) 2,3,4-TCP, (3) 3,5-DCP, (4) dichlorodihydroxy-benzene, (5) 3,4,5-trichlorocatechol, (6) 2,3,4,5-TeCP, and (7) 3,4,5-TCP ($[TeCP]_0$ = 5 mg/L, pH = 8).

This part of the study shows the potentialities of PdPc(Imz)/ITO/Glass as photocatalyst in water decontamination. This method requires only oxygen as a chemical reactant. For 2,3,4,5 TeCP, chosen as a model of chlorinated aromatic pollutants, the intermediate products such as TCP, DCP, and trichlorocatechol still remain after illumination. However, the complete degradation of the compounds requires much longer illumination time (t > 120 min). The chemical structure of intermediates with chlorine atoms and large number of hydroxyl groups should affect more significantly the photoreaction pathway than the hydroxyl groups from water. Furthermore, the degradation efficiency in this system depends on the film surface, and the degradation rate of a pollutant in low concentration can be decreased in the presence of more concentrated compounds by competition for the surface sites. This can be verified by comparing the decomposition of the four chlorophenols separately (Figure 8) with the simultaneous degradation (Figure 10), which generates numerous photochemical intermediates.

2.6.1. Effect of Ionic Strength on Photodegradation

In order to extrapolate our study to seawater, and quantify the contribution of PdPc(Imz) thin film in the photocatalytic degradation of chlorophenols, a series of experiments was conducted in artificial seawater to determine whether salinity (NaCl) and ionic-strength influence photodegradation. To determine the effects of salinity, laboratory experiments were conducted using 2,4-DCP as target compound. The chemical was dissolved in artificial seawater with varying NaCl concentrations. The red sea salinity varies slightly around 4%, which corresponds to 683 Mm [66]. We have therefore chosen this value as artificial seawater chloride concentration in our experiments. Three synthetic water matrices were created by mixing 5 mg/L of 2,4-DCP as a target compound in deionized water containing 20 mM phosphate buffer (pH 8) alone, with 683 mM $NaClO_4$ (ionic strength), or with 683 mM NaCl (seawater chloride). The degradation curves of 2,4-DCP in the synthetic matrices as a function of time are shown in Figure 12. It can be noted that compared to deionized water containing

20 mM phosphate buffer, photodegradation rates of 2,4-DCP were increased up to three fold in seawater chloride (683 mM NaCl). Furthermore, k_{obs} for 2,4-DCP increased from 153×10^{-3} min^{-1} in synthetic ionic strength matrix (683 mM $NaClO_4$) to 236×10^{-3} mn^{-1} in the deionized water matrix.

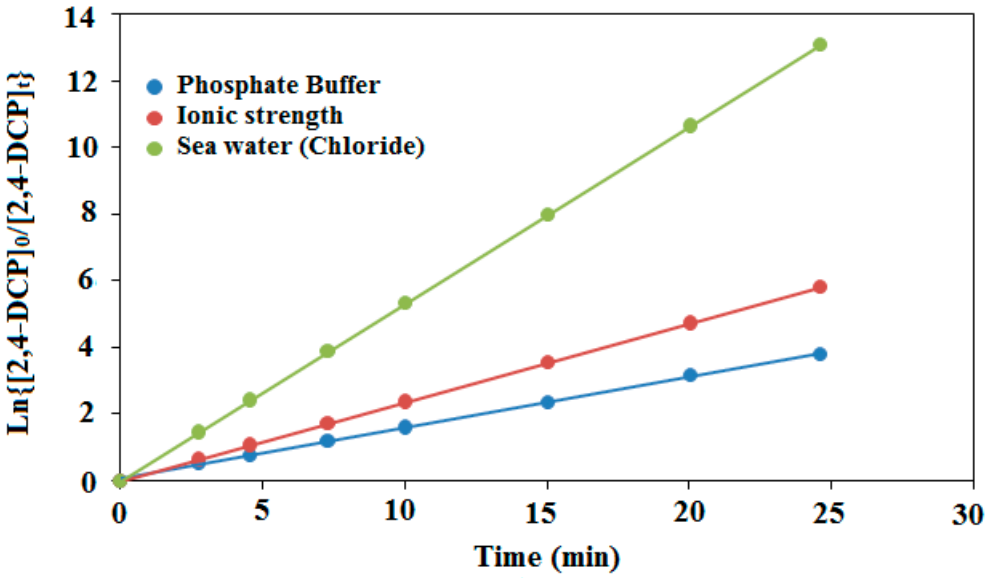


Figure 12. Photodegradation of 2,4-DCP target compound ($[2,4\text{-DCP}]_0$ = 5 mg/L) in synthetic sea water matrices containing 20 mM phosphate buffer alone at pH = 8, with 683 mM seawater (chloride), or with 683 mM $NaClO_4$ (ionic strength) after 30 min illumination time.

Quenching experiments including radical [•OH; 250 mM isopropanol], singlet oxygen [$^1O_2$; DABCO experiments], ^{3}[PdPc9(Imz)/ITO/glass]* electron transfer reactions (i.e., oxidation) [25 mM methanol as scavengers] resulted in ~10–50% reduction of 2,4-DCP photodegradation in seawater chloride (683 mM NaCl). Our results indicate that chlorides present in seawater increase the photodegradation of 2,4-DCP by a factor of 3. This could be attributed to photochemically generated chloride radicals, predominantly by direct oxidation of Cl^- by ^{3}PdPc9(Imz)/ITO/glass, according to the following reaction mechanism:

$$^3(PdPc9(Imz))^* + Cl^- \rightarrow {}^3(PdPc9(Imz))^{*-} + Cl^- \quad (7)$$

$$\rightarrow {}^3(PdPc9(Imz))^{*2-} \rightarrow (PdPc9(Imz))^{\bullet -} + Cl_2^{\bullet -} \quad (8)$$

The hydroxyl radicals can be also formed from Buxter reaction [67]:

$$Cl_2^{\bullet -} + HOH \rightarrow HOClH^{\bullet} + Cl^- \quad (9)$$

$$HOClH^{\bullet} \leftrightarrow H^+ + HOCl^{\bullet -} \quad (10)$$

$$HOCl^{\bullet -} \leftrightarrow Cl^- + {}^{\bullet}OH \quad (11)$$

These results indicate that chlorides increase the photodegradation of chlorophenols and modify its transformation pathway.

2.6.2. Concentration and Major Inorganic Ions Effect on Photodegradation Rate

A series of experiments were carried out to determine whether the major ion composition of seawater could affect the photocatalytic degradation rate of chlorophenols. To approximate the composition of the Red Sea, the results reported by Masoud et al. [68] were used to create the synthetic seawater solution employed to study the effect of the composition of other ions on the rate of

degradation of 2,4-DCP. Synthetic seawater containing 680 mM NaCl, 4.55 μM Na_2PO_4, 0.2 μM Iron, 1.29 μM KNO_3, and 1.49 mM $CaCO_3$ as total alkalinity were prepared using reagent-grade chemicals. Figure 13 shows the effect of seawater constituents on photodegradation rate in synthetic matrices of 2,4-DCP at initial concentration of 5 mg/L, compared to seawater chlorine 680 mM.

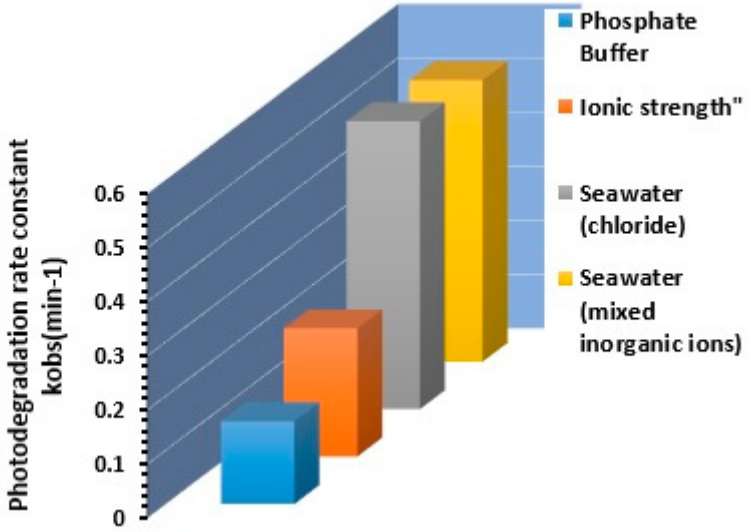


Figure 13. Effect of seawater constituents on photodegradation rate in synthetic matrices of 2,4-DCP at initial concentration of 5 mg/L, compared to seawater chlorine 680 mM.

2.7. Reusability of PdPc(Imz)/ITO/Glass Thin-Film

The reusability of the spent PdPc(Imz)/ITO/Glass thin film was examined to evaluate the photostability and effectiveness of the photocatalyst. The results revealed that PdPc(Imz)/ITO/Glass thin-film displayed very good photostability. Compared with powder catalyst, this film had the advantage of having low loss of photocatalytic activity after four cycling runs (see Supplementary Materials).

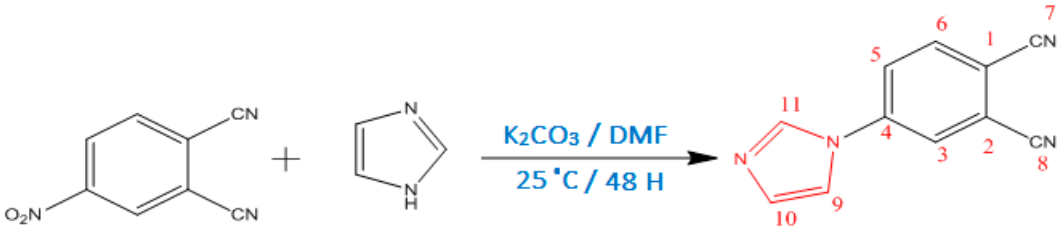
3. Materials and Methods

3.1. Materials

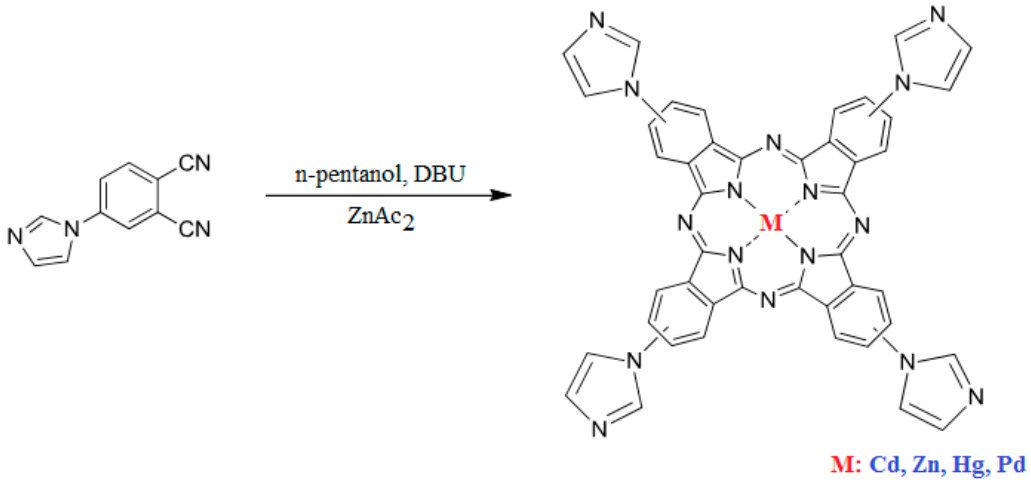
All reagents for synthesis were of analytical quality and used as such. The anhydrous metal salts [$Cd(OAc)_2$, $Hg(OAc)_2$, $Pd(OAc)_2$ and $Zn(OAc)_2$] and silver nitrate ($AgNO_3$) were purchased from Merck Co. Doubly distilled water was used everywhere. Dimethyl sulfoxide (DMSO), N, N-dimethylformamide (DMF), isopropyl alcohol, methanol, n-pentanol and 2-(dimethylamino) ethanol (DMAE) were purchased from Sigma-Aldrich (Germany). Standard materials for chlorinated phenols [2-chlrophenol (2-CP), (2,4-dichlorophenol (2,4-DCP), 2,4,6-trichlorophenol (2,4,6-TCP) and 2,3,4,5-tetrachlorophenol (2,3,4,5-TeCP)] were supplied by Supelco, 4-nitrophthalonitrile, DABCO (1,4-diazabicyclo [2.2.2] octane) and DBU (1,8-Diazabicyclo[5.4.0]undec-7-ene) were also obtained from Sigma-Aldrich. The phosphate buffer (pH = 8) used for the photocatalysis of chlorophenols was prepared using potassium dihygrogen orthophosphate reagent grade (Sigma-Aldrich) and dipotassium hydrogen phosphate (Sigma-Aldrich).

3.2. Synthesis

Synthetic pathways of the phthalonitrile and Pc derivatives are given in Schemes 1 and 2, respectively.



Scheme 1. Synthesis of 4-(1H-imidazol-1-yl)phthalonitrile.



Scheme 2. Structure of the synthesized compounds.

3.2.1. Synthesis of 4-(1H-imidazol-1-yl)phthalonitrile

The synthesis of 4-(1H-imidazol-1-yl)phthalonitrile was carried out by base-catalyzed aromatic nitro displacement of 4-nitrophthalonitrile with 1,3-Diaza-2,4-cyclopentadiene, in DMF; K_2CO_3 was used as the base for this displacement (Scheme 1).

3.2.2. Synthesis of the Phthalocyanines

The desired metallophthalocyanines were synthesized in a one-step reaction by cyclotetramerization of 4-(1H-imidazol-1-yl) phthalonitrile (3 mmol) in the presence of n-pentanol using DBU as the catalyst, in 2-(dimethylamino)ethanol (DMAE) under an inert atmosphere, at 140 °C for 18 h and stirred during one day to increase the yield (Scheme 2). We conducted the reaction in the presence of anhydrous metal salts [$Cd(OAc)_2$, $Hg(OAc)_2$, $Pd(OAc)_2$ and $Zn(OAc)_2$] (1 mmol) at reflux temperature. 1H NMR, MALDI-TOF-MS, and UV–Vis analyses confirmed the proposed structures of the synthesized compounds. All phthalocyanines displayed good solubility in DMSO, DMF, chloroform, and THF.

3.3. Preparation of Thin Films and Sensitization Process

Thin layers of the MPc(Imz) (M: Cd, Zn, Hg, Pd) have been prepared by a spin-coating technique on a glass substrate at 120 °C. The coating liquid was obtained by dissolving an adequate amount of MPc(Imz) to obtain a 5 mg/mL solution in a solvents mixture (Trifluoroacetic acid (TFA): Tetrahydrofuran (THF) = 1:1 in volume). Before deposition, substrates were cleaned by ultrasonication with acetone, isopropyl alcohol, and deionized water, followed by UV-ozone treatment. Finally, in the sensitization process, 1 mL of the coating solution was applied by spinning at a speed of 2000 rpm for 15 s in a closed spinner. These two parameters controlling the thickness of the resulting layers have been previously optimized by several tests to obtain the best crystalline structure. Afterwards, the resulting sensitized

film coatings were quickly placed in the oven set to 120 °C for 1 h to investigate the crystalline phase transition. Finally, the films are annealed at 200 °C temperature during 2 h.

3.4. Photocatalytic Experiments

In order to simulate contaminated sea water condition, synthetic seawater sample was spiked with appropriate amounts of stock solutions of a mixture of four chlorophenols. Based on previous works in our laboratory [26,27], photocatalytic degradation was achieved using a self-made designed photoreactor with slight modifications (Figure 14). A Lightex LT50 lamp with 128 W was used as a source of illumination and immersed in the reactor at a distance of 1 cm from the film supported on the ITO/glass substrate. Throughout the photocatalytic process, the solution enriched with chlorophenols was saturated with oxygen. The duration of illumination for each run was set at 140 min to ensure maximum degradation of the chlorinated phenols. 25 mL of mixed chlorophenols spiked in synthetic seawater solution (5 ppm) was used as target solution. The pH value of the batch reaction was fixed at 8.0 and the temperature in the photo-reactor set at 300 K with oxygen bubbling inside the reaction medium. At different intervals of illumination, a 5 mL aliquot containing the unreacted chlorophenols was taken and filtered through 0.45 µm cellulose esters (MCE) membrane (MF-Millipore). After acetylation and centrifugation, 1 µL aliquot of the organic phase was injected into the GC–MS system after pre-concentration and solid-phase extraction (SPE) clean-up procedure. The concentration of unreacted chlorophenols was determined to establish a calibration curve with concentration values ranging from 1 to 100 mg/L. For each test, three measurements were undertaken. Calibration curves showed good linearity with correlation coefficients (R^2) ranging from 0.9972 to 0.9998 for all the chlorophenols.

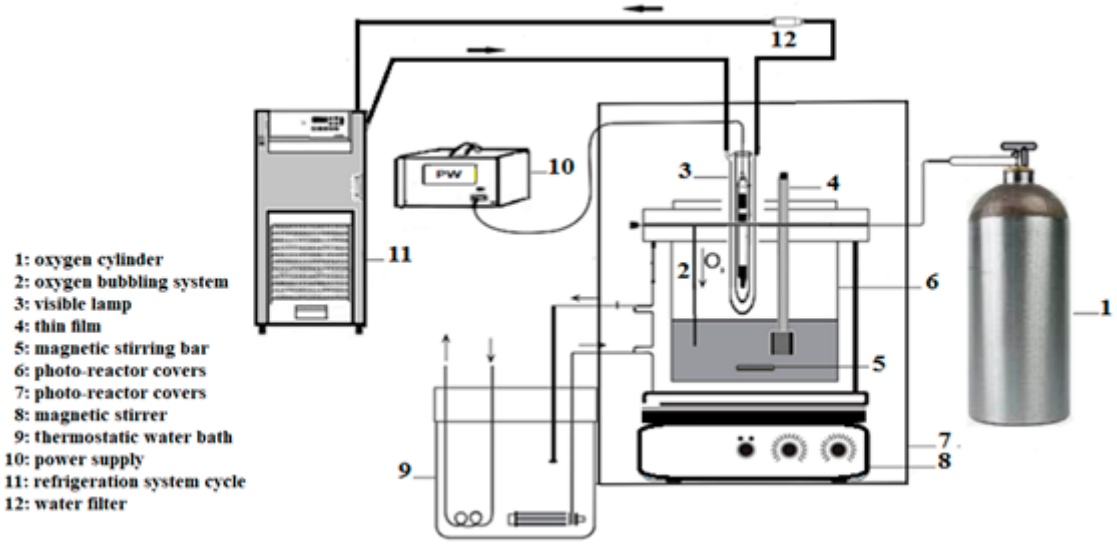


Figure 14. Scheme of the photo-oxidation experimental system.

4. Conclusions

In summary, a series of new metal phthalocyanines (CuPc, HgPc, ZnPc and PdPc) with imidazole function have been synthesized. These complexes were characterized with UV/VIS, FT-IR, and RMN^{1}H. All MPc(Imz) imidazole as well as their vibrational frequencies have been studied by DFT method using B3LYP theory level. The total energy and dipole moments of the studied molecules were also calculated. FTIR spectrum suggested that the PdMPc(Im) can be used as an important and promising catalyst for application in photocatalytic degradation under visible-light due to its band gap of ~2.76eV. Experimental results of MPcs studies were confirmed by numerical calculations by Gaussian W. HOMO-LUMO gaps, which have been determined for all ImzPCs (see Supplementary Materials). These numerical calculations of PdPc(Imz) values are close to the Uv-vis experimental results, indicating a semiconductor behavior. The surface morphology, crystal structure and electronic

properties of PdPc films on ITO glass have been also investigated. Based on the present study, the contribution of chloride radicals to the photochemical degradation of the critical organic compound may have important implications for decontamination of seawaters rich in chlorophenols, in the presence of a photosensitizer (e.g., PdPc(Imz)).

Supplementary Materials: The following are available online at http://www.mdpi.com/2073-4344/10/8/906/s1, FT-IR study of metallophthalocyanines (M: Zn(II), Cd (II), Hg(II) and Pd(II)), Numerical calculations by Gaussian of Palladium tetra (1H-imidazol-1-yl) Phtalocyanine, Effect of initial pH and initial concentration, Reusability of PdPc(Imz)/ITO/Glass thin-film.

Author Contributions: Conceptualization and photoreactor design, B.J. and R.C.; methodology, B.J. and R.C.; validation, B.J.; formal analysis, A.T.; investigation, data analysis, interpretation of experimental results, and original draft writing were carried out according to their specialties by B.J., R.C., A.T., and K.E.; writing—review and editing, R.C. and A.T.; supervision and project administration, B.J.; funding acquisition, B.J. All authors have read and agreed to the published version of the manuscript.

Funding: This project was funded by the Deanship of Scientific Research (DSR), King Abdulaziz University, Jeddah, under Grant No (DF-746-155-1441).

Acknowledgments: The authors gratefully acknowledge Deanship of Scientific Research (DSR), King Abdulaziz University, for technical and financial support.

Conflicts of Interest: The authors declare no conflict of interest.

References

1. Ge, F.; Zhu, L.; Wang, J. Distribution of chlorination products of phenols under various pHs in water disinfection. *Desalination* **2008**, *225*, 156–166. [CrossRef]
2. Hugo, H.; Santiesteban, L.; Rodríguez-Vázquez, R. Fungal degradation of organochlorine pesticides. In *Microbe-Induced Degradation of Pesticides*, 1st ed.; Singh, S.N., Ed.; Springer International Publishing AG: Cham, Switzerland, 2017; pp. 131–149. [CrossRef]
3. Igbinosa, E.O.; Odjadjare, E.E.; Chigor, V.N.; Igbinosa, I.H.; Emoghene, A.O.; Ekhaise, F.O.; Igiehon, N.O.; Idemudia, O.G. Toxicological profile of chlorophenols and their Derivatives in the Environment: The Public Health Perspective. *Sci. World J.* **2013**, 1–11. [CrossRef]
4. Adeola, A.O. Fate and toxicity of chlorinated phenols of environmental implications: A review. *Med. Anal. Chem. Int. J.* **2018**, *2*, 000126. [CrossRef]
5. Iwase, M.; Suzuki, A.; Akiyama, T.; Oku, T. Fabrication and Characterization of Phthalocyanine-Based Organic Solar Cells. *Mater. Sci. Appl.* **2014**, *5*, 278–284. [CrossRef]
6. Cole, A.; McIlroy, R.J.; Thorpe, S.C.; Cook, M.J.; McMurdo, J.; Ray, A.K. Substituted phthalocyanine gas sensors. *Sens. Actuat. B Chem.* **1993**, *13*, 416–419. [CrossRef]
7. Ayari, S.; Saglam, F.M.; Şenkuytu, E.; Erçin, P.B.; Zorlu, Y.; Sengul, I.F.; Jamoussi, B.; Atilla, D. 3-Methylindole-substituted zinc phthalocyanines for photodynamic cancer therapy. *J. Porphyr. Phthalocyanines* **2019**, *23*, 1371–1379. [CrossRef]
8. Kahouech, M.S.; Hriz, K.; Touaiti, S.; Jamoussi, B. New anthracene-based-phtalocyanine semi-conducting materials: Synthesis and optoelectronic properties. *Mater. Res. Bull.* **2016**, *75*, 144–154. [CrossRef]
9. Khalil, S.; Tazarki, H.; Mehdi, S.; Souli, M.; Guasch, C.; Jamoussi, B.; Kamoun, N. Synthesis and characterization of novel 4−Tetra-4-Tolylsulfonyl ZnPc thin films for optoelectronic applications. *Appl. Surf. Sci.* **2017**, *421*, 205–212. [CrossRef]
10. Durmuş, M.; Lebrun, C.; Ahsen, V. Synthesis and characterization of novel liquid and liquid crystalline phthalocyanines. *J. Porphyr. Phthalocyanines* **2004**, *10*, 1175–1186. [CrossRef]
11. Hoffmann, M.R.; Hong, A.P.K. Catalytic oxidation of reduced sulfur compounds by homogeneous and heterogeneous Co(II) phthalocyanine complexes. *Sci. Total Environ.* **1987**, *64*, 99–115. [CrossRef]
12. Naeimi, H.; Rahmatinejad, S. Nano magnetite supported phthalocyanine complexes of Cu(II) and Fe(II) as new heterogeneous effective catalysts for synthesis of β-amido ketones. *J. Coord. Chem.* **2018**, *71*, 4210–4227. [CrossRef]
13. Chatti, I.; Ghorbel, A.; Grange, P.; Colin, J.M. Oxidation of mercaptans in light oil sweetening by cobalt(II)phthalocyanine–hydrotalcite catalysts. *Catal. Today* **2002**, *75*, 113–117. [CrossRef]

14. Temizel, S.; Çanak, T.Ç.; Sevim, A.M. Novel polymers with cobalt(II)phthalocyanine moieties as effective heterogeneous photocatalysts for visible-light-driven photodegradation of organic dyes in aqueous solutions. *J. Photochem. Photobiol. A* **2020**, *401*, 112741. [CrossRef]
15. Que, L.; Tolman, W.B. Biologically inspired oxidation catalysis. *Nature* **2008**, *455*, 333–340. [CrossRef]
16. Mangematin, S.; Sorokin, A.B. Synthesis and catalytic properties of a novel phthalocyanine covalently grafted onto silica. *J. Porphyr. Phthalocyanines* **2001**, *5*, 674–680. [CrossRef]
17. Sehlotho, N.; Nyokong, T. Catalytic activity of iron and cobalt phthalocyanine complexes towards the oxidation of cyclohexene using tert-butylhydroperoxide and chloroperoxybenzoic acid. *J. Mol. Catal. A Chem.* **2004**, *209*, 51–57. [CrossRef]
18. Zalomaeva, O.V.; Ivanchikova, I.D.; Kholdeeva, O.A.; Sorokin, A.B. Kinetics and mechanism of the oxidation of alkyl substituted phenols and naphthols with tBuOOH in the presence of supported iron phthalocyanine. *New J. Chem.* **2009**, *33*, 1031–1037. [CrossRef]
19. Meunier, B.; Sorokin, A. Oxidation of Pollutants Catalyzed by Metallophthalocyanines. *Acc. Chem. Res.* **1997**, *30*, 470–476. [CrossRef]
20. Sorokin, A.; Fraisse, L.; Rabion, A.; Meunier, B. Metallophthalocyanine-catalyzed oxidation of catechols by H_2O_2 and its surrogates. *J. Mol. Catal. A Chem.* **1997**, *117*, 103–114. [CrossRef]
21. Hage, R.; Lienke, A. Applications of Transition-Metal Catalysts to Textile and Wood-Pulp Bleaching. *Angew. Chem. Int. Ed.* **2006**, *45*, 206–222. [CrossRef]
22. Sorokin, A.; Meunier, B.; Séris, J.L. Efficient oxidative dechlorination and aromatic ring cleavage of chlorinated phenols catalyzed by iron sulfophthalocyanine. *Science* **1995**, *268*, 1163–1166. [CrossRef] [PubMed]
23. Sorokin, A.; Meunier, B. Oxidative degradation of polychlorinated phenols catalyzed by metallosulfophthalocyanines. *Chem. Eur. J.* **1996**, *2*, 1308–1317. [CrossRef]
24. Sorokin, A.; De Suzzoni-Dezard, S.; Poullain, D.; Noèl, J.B.; Meunier, B. CO_2 as the Ultimate Degradation Product in the H_2O_2 Oxidation of 2,4,6-Trichlorophenol Catalyzed by IronTetrasulfophthalocyanine. *J. Am. Chem. Soc.* **1996**, *118*, 7410–7411. [CrossRef]
25. Hadasch, A.; Sorokin, A.; Rabion, A.; Fraisse, L.; Meunier, B. Oxidation of 2,4,6-trichlorophenol (TCP) catalyzed by iron tetrasulfophthalocyanine (FePcS) supported on a cationic ion-exchange resin. *Bull. Soc. Chim. Fr.* **1997**, *134*, 1025–1032. [CrossRef]
26. Smida, H.B.Y.; Jamoussi, B. Degradation of Nitroaromatic Pollutant by Titanium dioxide/Zinc Phthalocyanine: Study of the Influencing Factors. *J. Appl. Chem.* **2012**, *2*, 11–17. [CrossRef]
27. Smida, H.B.Y.; Beicheickh, M.; Jamoussi, B. Degradation of Hydroxytyrosol in Olive Oil Mill Wastewaters using Thermosensitive Zinc Phthalocyanine-Modified Titanium Dioxide. *J. Residuals Sci. Technol.* **2013**, *10*, 47–54.
28. Mele, G.; Del Sole, R.; Vasapollo, G.; García-López, E.; Palmisano, M.; Schiavello, M. Photocatalytic degradation of 4-nitrophenol in aqueous suspension by using polycrystalline TiO_2 impregnated with functionalized Cu(II)–porphyrin or Cu(II)–phthalocyanine. *J. Catal.* **2003**, *217*, 334–342. [CrossRef]
29. El-Khouly, M.E.; Rogers, L.M.; Zandler, M.E.; Suresh, G.; Fujitsuka, M.; Ito, O.; D'Souza, F. Studies on Intra-Supramolecular and Intermolecular Electron-Transfer Processes between Zinc Naphthalocyanine and Imidazole-Appended Fullerene. *Chem. Phys. Chem.* **2003**, *4*, 474–481. [CrossRef]
30. Derry, G.N.; Kern, M.E.; Worth, E.H. Recommended values of clean metal surface work functions. *J. Vac. Sci. Technol. A* **2015**, *33*, 060801. [CrossRef]
31. Kashiwaya, S.; Morasch, J.; Streibel, V.; Toupance, T.; Jaegermann, W.; Klein, A. The Work Function of TiO_2. *Surfaces* **2018**, *1*, 73–89. [CrossRef]
32. Xu, J.; Zhao, L.; Hou, W.; Guo, H.; Zhang, H. Dependence of morphology, substrate and thickness of iron phthalocyanine thin films on the photocatalytic degradation of rhodamine B dye. *Chem. Pap.* **2018**, *72*, 2327–2337. [CrossRef]
33. Chakane, S.; Datir, A.; Koinkar, P. Spin coated unsubstituted copper phthalocyanine thin films for nitrogen dioxide sensors. *Mod. Phys. Lett. B* **2015**, *29*, 1540032. [CrossRef]
34. Al-Raqa, S.Y.; Solieman, A.S.; Joraid, A.A.; Alamri, S.N.; Moussa, Z.; Aljuhani, A. Preparation and optical properties of novel symmetrical hexadecachlorinatedphthalocyaninato zinc (II) spin coated thin films. *Polyhedron* **2008**, *27*, 1256–1261. [CrossRef]

35. Critchley, S.M.; Willis, M.R. Deposition of thin phthalocyanine films by spin coating. *Int. J. Electron.* **1994**, *76*, 809–814. [CrossRef]
36. Karimi, A.R.; Khodadadi, A. Synthesis and solution properties of new metal-free and metallo-phthalocyanines containing four bis(indol-3-yl)methane groups. *Tetrahedron Lett.* **2012**, *53*, 5223–5226. [CrossRef]
37. De la Torre, G.; Nicolau, M.; Torres, T. Phtalocyanine: Synthesis, supramolecular organization and physical properties. In *Supramolecular Photosensitive and Electroactive Materials*; Singh, S.N., Ed.; Stanford Scientific Corporation: Los Angeles, CA, USA, 2001; pp. 1–111.
38. Claessens, C.G.; González-Rodríguez, D.; Torres, T. Subphthalocyanines: Singular nonplanar aromatic compounds synthesis, reactivity, and physical properties. *Chem. Rev.* **2002**, *102*, 835–853. [CrossRef]
39. Leznoff, C.C.; Vigh, S.; Svirskaya, P.I.; Greenberg, S.; Drew, D.M.; Ben-Hur, E.; Rosenthal, I. Synthesis and photocytotoxicity of some new substituted phthalocyanines. *Photochem. Photobiol.* **1989**, *49*, 279–284. [CrossRef]
40. Nyokong, T. Effects of substituents on the photochemical and photophysical properties of main group metal phthalocyanines. *Coord. Chem. Rev.* **2007**, *251*, 1707–1722. [CrossRef]
41. Lokesh, K.S.; Adriaens, A. Synthesis and characterization of Tetra-substituted palladium phthalocyanine complexes. *Dye. Pigm.* **2013**, *96*, 269–277. [CrossRef]
42. Raciti, R.; Bahariqushchi, R.; Summonte, C.; Aydinli, A.; Terrasi, A.; Mirabella, S. Optical band gap of semiconductor nanostructures: Methods for experimental data analysis. *J. Appl. Phys.* **2017**, *121*, 234304. [CrossRef]
43. Feng, Y.; Lin, S.; Huang, S.; Shrestha, S.; Conibeer, G. Can Tauc plot extrapolation be used for direct-band-gap semiconductor nanocrystals? *J. Appl. Phys.* **2015**, *117*, 125701. [CrossRef]
44. Murphy, A.B. Band-gap determination from diffuse reflectance measurements of semiconductor films, and application to photoelectrochemical water-splitting. *Sol. Energy Mater. Sol. Cells.* **2007**, *91*, 1326–1337. [CrossRef]
45. Enderby, J.E.; Barnes, A.C. Liquid semiconductors. *Rep. Prog. Phys.* **1990**, *53*, 85. [CrossRef]
46. El-Nhass, M.M.; Soliman, H.S.; Metwally, H.S.; Farid, A.M.; Farag, A.A.M.; El Shazly, A.A. Optical properties of evaporated iron phthalocyanine (FePc) thin films. *J. Opt.* **2001**, *30*, 121–129. [CrossRef]
47. Hamam, K.J.; Alomari, M.I. A study of the optical band gap of zinc phthalocyanine nanoparticles using UV–Vis spectroscopy and DFT function. *Appl. Nanosci.* **2017**, *7*, 261–268. [CrossRef]
48. Tauc, J.; Grigorovici, R.; Vancu, A. Optical Properties and Electronic Structure of Amorphous Germanium. *Phys. Status Solidi B* **1966**, *15*, 627–637. [CrossRef]
49. Timoumi, A.; Al Turkestani, M.K.; Alamri, S.N.; Alamri, H.; Ouerfelli, J.; Jamoussi, B. Synthesis and characterization of thin films of palladium (II) phthalocyanine and its derivatives using the thermal evaporation technique. *J. Mater. Sci. Mater. Electron.* **2017**, *28*, 7480–7488. [CrossRef]
50. Ghosh, M.; Jana, S.C. Fabrication of Hollow and Porous Tin-Doped Indium Oxide Nanofibers and Microtubes via a Gas Jet Fiber Spinning Process. *Materials* **2020**, *13*, 1539. [CrossRef]
51. Xue, M.; Jiang, Z.; Li, W.; Bi, G.; Ou, J.; Wang, F.; Li, C. Self-assembly growth and electron work function of copper phthalocyanine films on indium tin oxide glass. *Appl. Surf. Sci.* **2012**, *258*, 3373–3377. [CrossRef]
52. Kulkarni, A.K.; Schulz, K.H.; Lim, T.S.; Khan, M. Dependence of the sheet resistance of indium-tin-oxide thin films on grain size and grain orientation determined from X-ray diffraction techniques. *Thin Solid Film.* **1999**, *345*, 273–277. [CrossRef]
53. Griscom, D.L. Optical Properties and Struct. Defects Silica Glass. *J. Ceram. Soc. Jpn.* **1991**, *99*, 923–942. [CrossRef]
54. Ahn, S.; Jeong, S.H.; Han, T.H.; Lee, T.W. Conducting Polymers as Anode Buffer Materials in Organic and Perovskite Optoelectronics. *Adv. Opt. Mater.* **2016**, 1–24. [CrossRef]
55. Kim, H.K.; Kang, S.J. Effective Work Function Control of Indium-tin-oxide Electrodes. *J. Korean Phys. Soc.* **2011**, *59*, 2655–2657. [CrossRef]
56. Tadjarodi, A.; Hossein, A.; Khavar, C.; Imani, M. The removal of 2,4-dichlorophenol under visible light irradiation by silver indium sulfide nanoparticles synthesized by microwave. *Curr. Chem. Lett.* **2013**, *2*, 77–84. [CrossRef]
57. Pirbazari, A.E. Photocatalytical treatment of synthetic wastewater containing chlorophenols by TiO_2 nanoparticles sensitized with cobalt phthalocyanine under visible light. *J. Chem. Eng. Process. Technol.* **2017**, *8*. [CrossRef]

58. Hajimohammadi, M.; Sereshk, A.V.; Schwarzinger, C.; Knör, G. Suppressing Effect of 2-Nitrobenzaldehyde on Singlet Oxygen Generation, Fatty Acid Photooxidation, and Dye-Sensitizer Degradation. *Antioxidants* **2018**, *7*, 194. [CrossRef]
59. Czaplicka, M.; Czaplicki, A. Photodegradation of 2,3,4,5-tetrachlorophenol in water/methanol mixture. *J. Photochem. Photobiol. A* **2006**, *178*, 90–97. [CrossRef]
60. Boule, P.; Guyon, C.; Tissot, A.; Lemaire, J. Specific phototransformation of xenobiotic compounds: Chlorobenzenes and halophenols. In *Photochemistry of Environmental Aquatic Systems*; Zika, R.G., Cooper, W.J., Eds.; American Chemical Society: Washington, DC, USA, 1987; Volume 327, pp. 10–26.
61. D'Oliveira, J.C.; Al-Sayyed, G.; Pichat, P. Photodegradation of 2- and 3-Chlorophenol in TiO_2 Aqueous Suspensions. *Environ. Sci. Technol.* **1990**, *24*, 990–996. [CrossRef]
62. Bashiri, H.; Rafiee, M. Kinetic Monte Carlo simulation of 2,4,6-thrichloro phenol ozonation in the presence of ZnO nanocatalyst. *J. Saudi Chem. Soc.* **2016**, *20*, 474–479. [CrossRef]
63. Saritha, P.; Raj, D.S.S.; Aparna, C.; Laxmi, P.N.V.; Himabindu, V.; Anjaneyulu, Y. Degradative oxidation of 2,4,6 trichlorophenol using advanced oxidation processes a comparative study. *Water Air Soil Pollut.* **2009**, *200*, 169–179. [CrossRef]
64. Chaliha, S.; Bhattacharyya, K.G. Wet oxidative method for removal of 2,4,6-trichlorophenol in water using Fe(III), Co(II), Ni(II) supported MCM41 catalysts. *J. Hazard. Mater.* **2008**, *150*, 728–736. [CrossRef] [PubMed]
65. Ji, H.; Chang, F.; Hu, X.; Qin, W.; Shen, J. Photocatalytic degradation of 2,4,6-trichlorophenol over g-C_3N_4 under visible light irradiation. *Chem. Eng. J.* **2013**, *218*, 183–190. [CrossRef]
66. Mezger, E.M.; De Nooijer, L.J.; Boer, W.; Brummer, G.J.A.; Reichart, G.J. Salinity controls on Na incorporation in Red Sea planktonic foraminifera. *Paleoceanogr. Paleoclimatol.* **2016**, *31*, 1562–1582. [CrossRef]
67. Buxter, G.V.; Bydder, M.; Salmon, G.A.; Williams, J.E. The reactivity of chlorine atoms in aqueous solution. Part III. The reactions of $Cl^{\bullet}$ with solutes. *Phys. Chem. Chem. Phys.* **2000**, *2*, 237–245. [CrossRef]
68. Masoud, M.S.; Abdel-Halim, A.M.; El Ashmawy, A.A. Seasonal variation of nutrient salts and heavy metals in mangrove (*Avicennia marina*) environment, Red Sea, Egypt. *Environ. Monit. Assess.* **2019**, *191*, 425. [CrossRef] [PubMed]



© 2020 by the authors. Licensee MDPI, Basel, Switzerland. This article is an open access article distributed under the terms and conditions of the Creative Commons Attribution (CC BY) license (http://creativecommons.org/licenses/by/4.0/).